

Re-Os geochronology and coupled Os-Sr isotope constraints on the Sturtian snowball Earth

Alan D. Rooney^{a,1}, Francis A. Macdonald^a, Justin V. Strauss^a, Francis Ö. Dudás^b, Christian Hallmann^{b,c,d}, and David Selby^e

^aDepartment of Earth and Planetary Sciences, Harvard University, Cambridge, MA 02138; ^bDepartment of Earth, Atmospheric and Planetary Sciences, Massachusetts Institute of Technology, Cambridge, MA 02139; ^cMax-Planck-Institute for Biogeochemistry, 07745 Jena, Germany; ^dCenter for Marine Environmental Sciences (MARUM), University of Bremen, 28359 Bremen, Germany; and ^eDepartment of Earth Sciences, Durham University, Durham DH1 3LE, United Kingdom

Edited* by Paul F. Hoffman, University of Victoria, Victoria, Canada, and approved November 8, 2013 (received for review June 21, 2013)

After nearly a billion years with no evidence for glaciation, ice advanced to equatorial latitudes at least twice between 717 and 635 Mya. Although the initiation mechanism of these Neoproterozoic Snowball Earth events has remained a mystery, the broad synchronicity of rifting of the supercontinent Rodinia, the emplacement of large igneous provinces at low latitude, and the onset of the Sturtian glaciation has suggested a tectonic forcing. We present unique Re-Os geochronology and high-resolution Os and Sr isotope profiles bracketing Sturtian-age glacial deposits of the Rapitan Group in northwest Canada. Coupled with existing U-Pb dates, the postglacial Re-Os date of 662.4 ± 3.9 Mya represents direct geochronological constraints for both the onset and demise of a Cryogenian glaciation from the same continental margin and suggests a 55-My duration of the Sturtian glacial epoch. The Os and Sr isotope data allow us to assess the relative weathering input of old radiogenic crust and more juvenile, mantle-derived substrate. The preglacial isotopic signals are consistent with an enhanced contribution of juvenile material to the oceans and glacial initiation through enhanced global weatherability. In contrast, postglacial strata feature radiogenic Os and Sr isotope compositions indicative of extensive glacial scouring of the continents and intense silicate weathering in a post-Snowball Earth hothouse.

renewal-oscium geochronology | strontium isotopes | osmium isotopes | Windermere Supergroup | Neoproterozoic glaciation

The Snowball Earth hypothesis predicts that Neoproterozoic glaciations were global and synchronous at low latitudes and that deglaciation occurred as a result of the buildup of $p\text{CO}_2$ to extreme levels resulting in a “greenhouse” aftermath (1, 2). The temporal framework of Cryogenian glaciations is built on chronostratigraphy and correlation of lithologically distinct units, such as glaciogenic deposits, iron formation, and cap carbonates (3), tied to the few successions that contain volcanic rocks dated using U-Pb zircon geochronology (4). In strata lacking horizons suitable for U-Pb geochronology, Re-Os geochronology can provide depositional ages on organic-rich sedimentary rocks bracketing glaciogenic strata (5, 6). Moreover, Os isotope stratigraphy can be used as a proxy to test for supergreenhouse weathering during deglaciation (7). In a Snowball Earth scenario, we can make specific predictions for Cryogenian weathering: CO_2 consumption via silicate weathering should increase before glaciation, stagnate during the glaciation, and increase again during deglaciation. However, the use of a single weathering proxy to provide evidence for such a scenario, such as Sr isotopes from marine carbonates, is limited both by lithological constraints and an inability to distinguish between the amount of weathering and the composition of what is being weathered (8). The short residence time of Os in the present-day oceans (<10 ky) (9) provides a complementary higher resolution archive to Sr isotopes, and thus, insights into the nature of extreme fluctuations in the Earth’s climate as documented herein.

Stratigraphy of the Neoproterozoic Windermere Supergroup

The Neoproterozoic Windermere Supergroup is spectacularly exposed in the Mackenzie Mountains of northwest Canada and comprises an ~7-km-thick mixed carbonate and siliciclastic marine succession (Fig. 1 and Fig. S1). The Coates Lake Group of the Mackenzie Mountains forms the base of the Windermere Supergroup and consists of siliciclastic, carbonate, and evaporitic strata of the Thundercloud, Redstone River, and Coppercap formations. The Coates Lake Group unconformably overlies the Little Dal basalt, which has been correlated geochemically with the Tsezotene sills (10), a 777 ± 2.5 – 1.8 Mya ($^{206}\text{Pb}/^{238}\text{U}$ multigrain zircon thermal ionization MS date) quartz diorite plug near Coates Lake (11), and the ~780-Mya Gunbarrel magmatic event (12).

Near Coates Lake, the Coppercap Formation is ~410 m thick and is separated into six units (CP1–CP6 in Fig. 2). The Coppercap Formation culminates with a partially dolomitized unit of carbonate conglomerate, with minor sandstone, chert, and evaporite (CP6), and is overlain by siltstone and diamictite of the Rapitan Group (Fig. 2). Economic copper deposits grading 3.9% occur in unit CP1 of the Coppercap Formation in a 1-m-thick interval (13, 14). These deposits formed directly below the flooding surface at the base of CP2 (14). Above this, in units CP2–CP5, there is no evidence for mineralization, exposure, or significant sulfate reduction, although minor evaporite and metal

Significance

The causal mechanisms of global glaciations are poorly understood. The transition to a Neoproterozoic Snowball Earth after more than 1 Gy without glaciation represents the most dramatic episode of climate change in the geological record. Here we present new Re-Os geochronology, which, together with existing U-Pb ages, reveal that the glacial period in northwest Canada lasted ~55 My. Additionally, we present an original method to track tectonic influences on these climatic perturbations with a high-resolution coupled Os-Sr isotope curve across the transition from an ice-free world to a Neoproterozoic Snowball Earth. The data indicate that increases in mantle-derived, juvenile material emplaced onto continents and subsequently weathered into the oceans led to enhanced consumption and sequestration of CO_2 into sediments.

Author contributions: F.A.M. and J.V.S. designed research; A.D.R., F.A.M., J.V.S., F.Ö.D., and C.H. performed research; A.D.R., F.A.M., F.Ö.D., C.H., and D.S. contributed new reagents/analytic tools; A.D.R., F.A.M., J.V.S., F.Ö.D., C.H., and D.S. analyzed data; and A.D.R., F.A.M., J.V.S., F.Ö.D., and D.S. wrote the paper.

The authors declare no conflict of interest.

*This Direct Submission article had a prearranged editor.

¹To whom correspondence should be addressed. E-mail: alanrooney@fas.harvard.edu.

This article contains supporting information online at www.pnas.org/lookup/suppl/doi:10.1073/pnas.1317266110/-DCSupplemental.

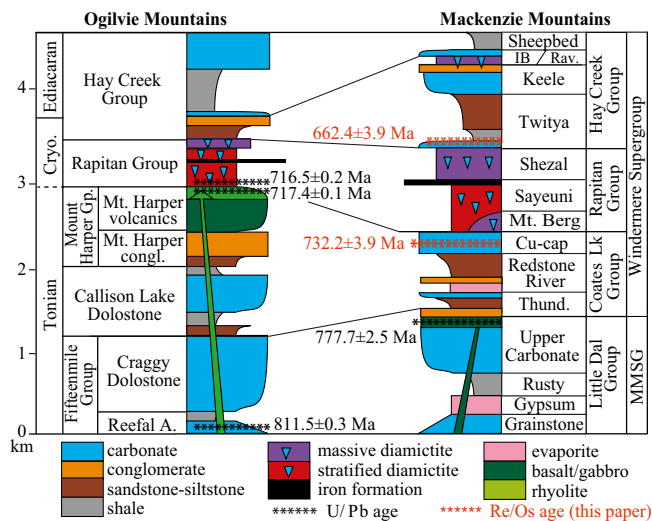


Fig. 1. Schematic of the Mackenzie and Ogilvie Mountains, Canada. U-Pb ages are from ref. 4 and Re-Os ages are from this work. Congl., conglomerate; Cryo., Cryogenian; Cu-cap, Coppercap Formation; Gp., Group; IB, Ice Brook Formation; Lk, Lake; Mt., Mount; Rav., Ravensthorpe formation; Reefal A., Reefal Assemblage; Thund., Thundercloud Formation.

showings are present in association with the exposure surfaces at the top of unit CP6.

Regionally, the Rapitan Group rests unconformably on the Coates Lake Group, but locally the contact can be gradational (15). In the Ogilvie Mountains, the age of the Rapitan Group is constrained by a $^{206}\text{Pb}/^{238}\text{U}$ single grain chemical abrasion-isotope dilution-thermal ionization MS (CA-ID-TIMS) zircon date of 717.4 ± 0.1 Mya on a rhyolite from the underlying Mount Harper volcanics and 716.5 ± 0.2 Mya on a volcanic tuff within the overlying glaciogenic diamictites, indicating that glaciation commenced ~ 717 Mya (4). The Rapitan Group is composed of three formations consisting of stratified and massive glaciogenic diamictites with minor iron formation (16, 17). The lowest unit, the Mount Berg Formation, is present only in the southern Mackenzie Mountains. The overlying Sayunei Formation is locally more than 600 m thick and comprises ferruginous, maroon to dark brown turbiditic siltstone, sandstone, debris, and intervals of stratified and massive glacial diamictite with dropstones of carbonate, basalt and rare granitoid clasts (16, 17). Discontinuous lenticular bodies of hematite-jaspillite iron formation are present near the top of the Sayunei Formation when they are not eroded by the overlying Shezal Formation (17, 18). The uppermost unit of the Rapitan Group, the Shezal Formation, consists of >600 m of green-gray, yellow weathering stratified and massive glacial diamictite interbedded with decimeter-scale units of mudstone, siltstone and sandstone, which in some localities unconformably overlies the Sayunei Formation (11, 15, 19). Clast composition in the Shezal Formation is highly variable with an abundance of carbonate, altered basic volcanic, sandstone, chert, and less common metamorphic pebbles and cobbles (16, 17). An extended duration for deposition of the Rapitan Group is supported by internal unconformities and paleomagnetic poles that shift $\sim 40^\circ$ from the Mount Berg to Sayunei Formations (20).

Locally, the basal Twitya Formation of the Hay Creek Group conformably overlies the Rapitan Group, but regionally various parts of the Twitya Formation rest unconformably on underlying strata (19). Where conformable, such as at Mountain River, the basal Twitya Formation consists of a 0- to 40-m-thick “cap carbonate” that is characterized by finely laminated lime mudstone and siltstone with minor graded beds and sedimentary slump folds

(Fig. 2). The lower Twitya Formation is part of a transgressive sequence that passes upward into fetid, pyritic black shale and then into hundreds of meters of gray-green siltstone and sandstone turbidites. These strata are succeeded by variable siliciclastic and carbonate strata of the Keele Formation and glaciogenic deposits of the Stelfox Member of the Ice Brook Formation. The Stelfox Member consists of massive diamictite with striated clasts (21) and is capped by the Ravensthorpe formation, a white to buff-colored dolostone (17, 22), which hosts sedimentological and geochemical features characteristic of globally distributed ~ 635 Mya Marinoan cap carbonates (2, 23).

Re-Os Geochronology

Organic-lean (<0.5% Total Organic Carbon; TOC) cryptalgal laminites of the Coppercap Formation were obtained from drill core and outcrop near Coates Lake (Figs. 1 and 2). Core samples were analyzed for major and minor elements, carbonate content, and C, Sr, and Os isotope chemostratigraphy, and four samples were used for Re-Os geochronology and Os isotope stratigraphy (see *SI Materials and Methods* for details).

A Re-Os age of 732.2 ± 3.9 Mya [4.7 Mya including ^{187}Re decay constant uncertainty, $n = 4$, mean square of weighted deviates (MSWD) = 1.9, 2σ , initial $^{187}\text{Os}/^{188}\text{Os} = 0.15 \pm 0.002$] was obtained from unit CP4 of the Coppercap Formation (Fig. 3A). In conjunction with existing U-Pb zircon ages from the Ogilvie Mountains, this Re-Os age indicates an interval ~ 15 My

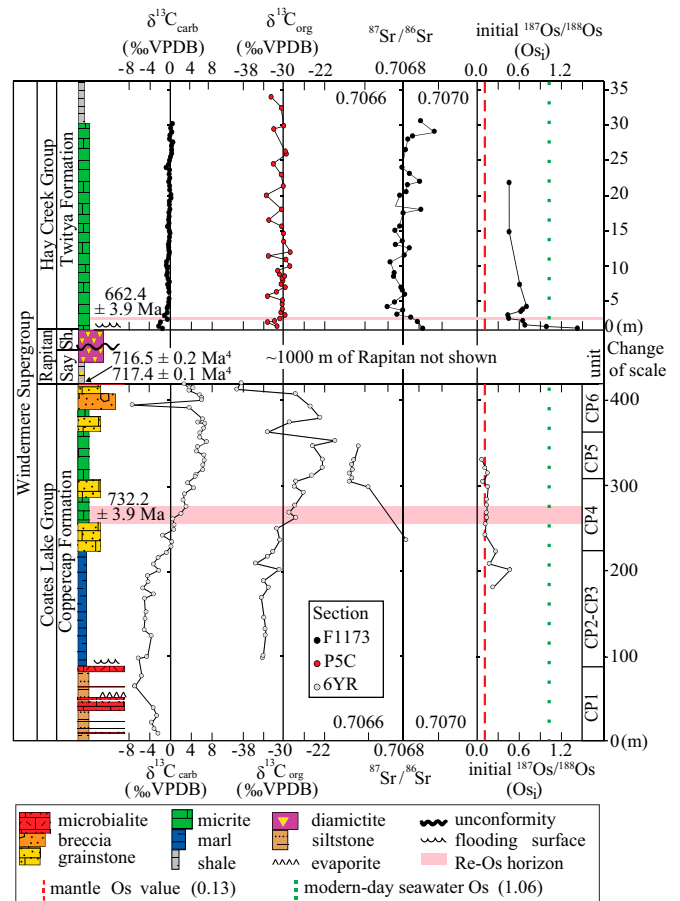


Fig. 2. Composite chemo- and lithostratigraphy of the Windermere Supergroup from the Mackenzie Mountains, Canada (measured sections F1173, P5C, and 6YR). Organic carbon isotope data for the Twitya Formation in Section P5C is from ref. 24. Say, Sayunei; Sh, Shezal. The superscript next to 716 and 717 Ma corresponds to the cited reference.

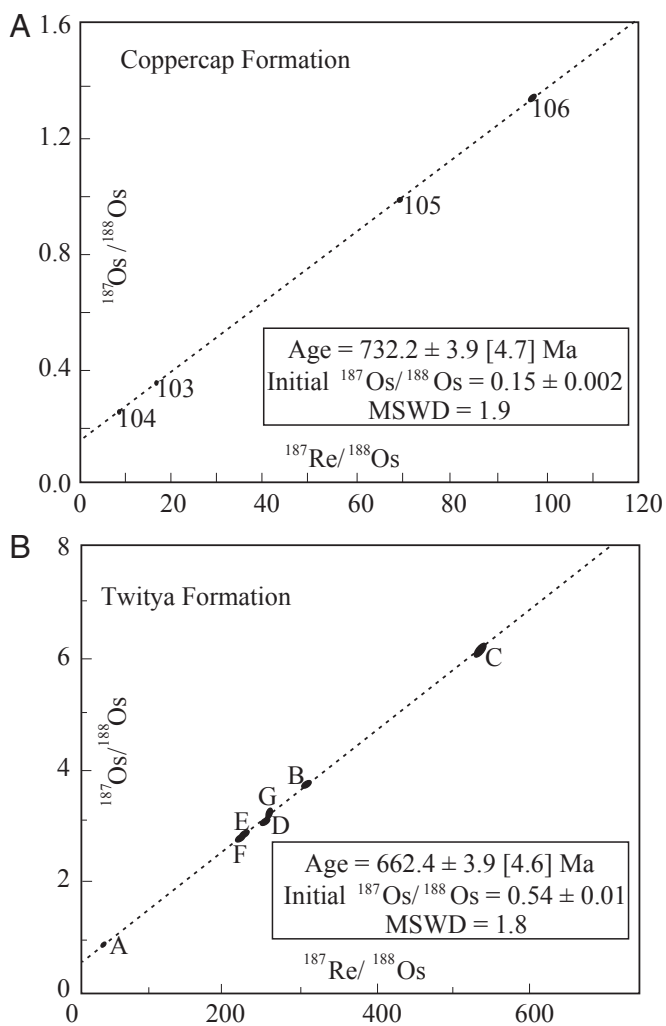


Fig. 3. (A) Re-Os isochron for the Coppercap Formation with an age uncertainty of 4.7 Mya when the uncertainty in the ^{187}Re decay constant is included. (B) Re-Os isochron for the Twitya Formation with an age uncertainty of 4.6 Mya when the uncertainty in the ^{187}Re decay constant is included. Isotope composition and abundance data are presented in Table S2.

between deposition of unit CP4 of the Coppercap Formation and Rapitan Group glaciogenic strata (Figs. 1 and 2).

Organic-rich (>0.5% TOC) micritic limestone of the post-glacial basal Twitya Formation was sampled from outcrop near Mountain River (64°32'04"N, 129°23'42"W). The cap limestone was sampled at ~0.5-m resolution for Sr, Os, and C isotope chemostratigraphy (24), and a thin (<20 cm) horizon less than 2 m above the Rapitan-Twitya contact was sampled for Re-Os geochronology (Fig. 2). The basal Twitya Formation yielded a Re-Os age of 662.4 ± 3.9 Mya (4.6 Mya including ^{187}Re decay constant uncertainty, $n = 7$, MSWD = 1.9, 2σ , initial $^{187}\text{Os}/^{188}\text{Os} = 0.54 \pm 0.01$; Fig. 3B). The 662.4 ± 3.9 Mya Re-Os date for the Twitya Formation together with the CA-ID-TIMS zircon date of 716.5 ± 0.2 Mya from the nearby Ogilvie Mountains (4) represents a crucial set of age constraints that date both the onset and demise of a Cryogenian glaciation from the same continental margin. Correlation of the Rapitan Group from the Yukon to the Northwest Territories (NWT) is supported not only by the bracketing stratigraphy but also by the presence of iron formation (25, 26) and paleomagnetic studies that link Rapitan poles from the NWT with the 723–716 Mya Franklin large igneous

province (20, 27), which was coeval with Rapitan glaciation in the Yukon (4).

Coupled Os and Sr Isotope Stratigraphy

The Os and Sr isotope compositions of seawater have been interpreted to reflect an input balance between radiogenic sources (weathering of upper continental crust and riverine input) and unradiogenic sources (cosmic dust, hydrothermal alteration of oceanic crust, and weathering of mafic or ultramafic rocks) (28). However, Os and Sr have distinct sources and sinks, are sensitive to varying geological processes, and have contrasting residence times. Therefore, combining these two weathering proxies to investigate Neoproterozoic climatic fluctuations represents a unique method to elucidate the relationship between increased rates of continental weathering and global climate change.

Initial $^{187}\text{Os}/^{188}\text{Os}$ (Os_i) values from the preglacial Coppercap Formation become increasingly unradiogenic up-section from a value of 0.24 to a nadir of 0.12 before Rapitan Group deposition (Fig. 2). This extremely low Os_i value is substantially less radiogenic than values reported for modern seawater ($^{187}\text{Os}/^{188}\text{Os} = 1.06$) (28) and is closer to the primitive upper mantle Os isotope composition ($732 \text{ Mya} = ^{187}\text{Os}/^{188}\text{Os} = 0.124$) (29). Although it is possible that episodic restriction within the Coates Lake basin, potential hydrothermal input, and/or weathering of a proximal ultramafic body may have contributed to the unradiogenic Os_i values in the Coppercap Formation (Fig. 2), units CP2–CP6 have been previously interpreted to have been deposited in an open marine embayment (14, 30).

In the Coppercap Formation, Sr isotope values are extremely scattered in units CP1–CP3 between 0.7169 and 0.7064, less scattered in units CP4 and CP5 with values converging between 0.7064 and 0.7066, and scattered again in unit CP6. In the Twitya Formation, Sr isotope values decline from 0.7069 to 0.7067 in the basal 5 m and continue to oscillate between 0.7068 and 0.7070 over the ensuing 20 m (Fig. 2 and Table S1).

Unlike the Phanerozoic marine Sr isotope curve, whose fidelity can be evaluated by comparisons between several sample types (31), Neoproterozoic marine Sr chemostratigraphy relies exclusively on analyses of whole rock carbonate samples that have potentially been subjected to a variety of diagenetic processes. Based on data from sequential dissolution experiments (32), Sr isotopic analyses of whole rock carbonate samples can be expected to vary in the fourth decimal place, i.e., the external reproducibility of “replicates” from the same sample is ± 0.0001 . Sr isotope measurements are commonly vetted for reliability with Mn/Sr, Sr/Ca, Rb/Sr, and Sr concentration. Mn/Sr is thought to be a sensitive indicator of alteration due to the increase in Mn and decrease of Sr during meteoric alteration (33, 34); however, we find that Mn/Sr and Rb/Sr ratios scale inversely with carbonate content (Table S1), likely reflecting the contamination of small amounts of Sr from clay minerals. Consequently, we cull unreliable results with both low carbonate content and Sr abundance. Above 90% carbonate content and Sr concentrations >650 ppm, $^{87}\text{Sr}/^{86}\text{Sr}$ scatter above 0.708 is eliminated. However, for samples with $^{87}\text{Sr}/^{86}\text{Sr}$ between 0.7064 and 0.7080 there is no dependence on carbonate content, Sr concentration, Mn/Sr, Rb/Sr, or Sr/Ca (Table S1). The lowest and most stratigraphically coherent and reproducible values are in units CP4 and CP5 and in the Twitya Formation. We thus consider these $^{87}\text{Sr}/^{86}\text{Sr}$ measurements as the most reliable (Fig. 2 and Table S1).

The lower Coppercap Formation (units CP1–CP3) contains detrital components derived from the Little Dal Basalt and siliciclastic strata of the Katherine Group (14). These strata have also been geochemically modified by basin-dewatering brines that were responsible for formation of the Coates Lake sediment-hosted Cu deposit. We interpret the radiogenic $^{87}\text{Sr}/^{86}\text{Sr}$ of the lower Coppercap Formation to reflect effects of both

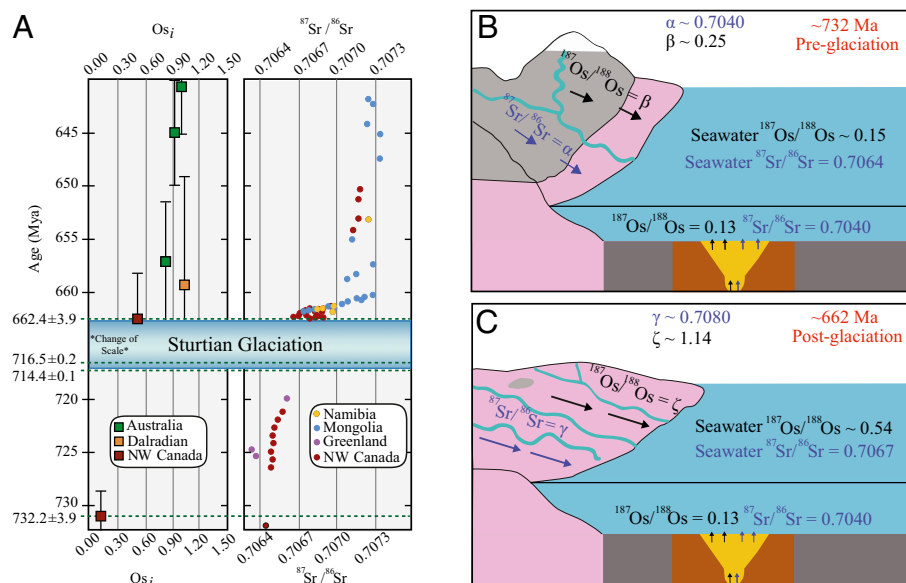


Fig. 4. (A) Compilation of initial $^{187}\text{Os}/^{188}\text{Os}$ isotope data and $^{87}\text{Sr}/^{86}\text{Sr}$ data for pre- and post-Sturtian successions worldwide (5, 6, 40, 53, 70). All data are in Tables S1–S5. (B) Geological cartoon of Neoproterozoic preglacial weathering fluxes. (C) Geological cartoon of postglacial weathering fluxes. See text and *SI Materials and Methods* for further details.

a higher siliciclastic component and potential postdepositional modification by basin-dewatering brines.

Duration and Synchronicity of the Sturtian Glacial Epoch

The Twitya Formation Re-Os date is identical, within uncertainty, to existing postglacial U-Pb zircon geochronological data from Australia and South China (Fig. 4, Fig. S2, and Table S6) (35, 36), although there are some discrepancies related to analytical procedures of some of the Re-Os ages from Australia (5, 6). Previous work yielded Re-Os age constraints for the Tindelpina Formation (6), which is an amalgamated date based on Re-Os data from two separate drill cores (SCYW-1a and Blinman-2) separated by >100 km. These two horizons were correlated using low-resolution $\delta^{13}\text{C}$ stratigraphy, which is not an accurate technique for sample selection for Re-Os geochronology. The four-point SCYW1a isochron in their study (6) contains two data points (a3-4 and a3-4r; Table S5) (supplemental data of ref. 6) that are actually two analyses of a single sample suggesting extreme sample heterogeneity. Due to these complications, we consider the SCYW1a age to be misleading and not suitable for global correlation.

A Re-Os date of 640.7 ± 4.7 Mya from Tasmanian organic-rich rocks has also been used to dispute the synchronicity of the Rapitan-Sturtian deglaciation (5). However, this date from the upper Black River Formation is located stratigraphically above two diamictite units that are separated by a carbonate unit and is overlain by the ~580-Mya Gaskiers-age Croles Hill diamictite (37). The Croles Hill diamictite was previously correlated with the Marinoan Cottons Breccia on King Island and the Elatina Formation in the Flinders Range of Australia, which implied that the upper Black River Formation was Sturtian in age. However, a new $^{206}\text{Pb}/^{238}\text{U}$ zircon CA-ID-TIMS date of 636.41 ± 0.45 Mya from the Cottons Breccia (23) suggests that the 640.7 ± 4.7 -Mya Re-Os age in the upper Black River Formation is instead correlative with the ~635-Mya Marinoan glaciation.

The glaciogenic Port Askaig Formation of the Dalradian Supergroup, Scotland, was deposited on the northeast margin of Laurentia and has been correlated with the Sturtian glaciation using lithostratigraphic and chemostratigraphic techniques (38, 39). A Re-Os age of 659.6 ± 9.6 Mya for the Ballachulish Slate

near Loch Leven (40) has been cited as a maximum age constraint for the Port Askaig Formation; however, the Port Askaig is not present in the region, and the relationship of the date to glaciogenic strata relies on regional correlations. A variety of tests on samples from the Ballachulish Slate indicate that the 659.6 ± 9.6 -Mya age represents a depositional age and not a mixed age from later metamorphic events (40). Therefore, if we assume that the ages on the Ballachulish and Twitya formations are robust, we are left with the following alternatives: (i) these dates are constraining two separate glaciations during the “Sturtian glacial epoch,” and these ages bracket the later event; (ii) the Sturtian glaciation is not preserved on the eastern margin of Laurentia, and the Port Askaig Formation represents the younger (~635 Mya) Marinoan glaciation and is correlative with the Stralinchy diamictite; or (iii) the Kinlochlaggan Boulder Bed is correlative with the Port Askaig Tillite as originally suggested by refs. 41 and 42. As a result, the Ballachulish Slate near Loch Leven would lie in the Argyll Group. Ultimately, additional tests of regional correlations and geochronological constraints are necessary to more fully resolve the complexities of the Dalradian Supergroup.

Existing $^{206}\text{Pb}/^{238}\text{U}$ zircon ages from Idaho have been previously used to argue that the Sturtian glaciation is globally diachronous (43, 44). However, these ages, coupled with the 711.5 ± 0.3 -Mya age from the Gubrah Formation in Oman (45), can also be interpreted to be syn-glacial constraints and correlative with the 717- to 662-Mya Sturtian glacial epoch recorded in northwest Canada (Fig. 4). Additional constraints from U-Pb and Re-Os geochronology are necessary to determine whether Sturtian glacial strata represent a series of glacial–interglacial cycles (46), a Jormagund climate state (47), or a continuous ~55-My Snowball Earth event.

It has also been suggested that there was an earlier, ~750-Ma glaciation recorded on the Kalahari (48), Congo (49), and Tarim (50) cratons. However, there is no direct evidence for glaciation in Kaigas Formation on the Kalahari Craton (51), and the ages from the Congo and Tarim cratons suffer from inheritance and cannot be relied on (see concordia diagrams in refs. 49 and 50). Our Re-Os age of 732.2 ± 3.9 Mya on the Coppercap Formation coupled with global C and Sr isotope correlation is consistent

with the lack of evidence for a pre-717-Mya glaciation. The large negative carbon isotope anomaly in the lower Coppercap Formation covaries in carbonate carbon and organic carbon isotopes (Fig. 2) and can be correlated with the Islay anomaly in Scotland, Greenland, and Svalbard (3). It is also consistent with pre-Sturtian Sr isotope values (52, 53). However, the Islay anomaly in Scotland is not present in the Loch Leven region in Scotland, and its relationship to the dated Ballachulish Slate (40) is unclear. The Re-Os geochronology presented here suggests that the Islay anomaly returns to positive $\delta^{13}\text{C}_{\text{carb}}$ values by ~ 732 Mya, well before the onset of glaciation at ~ 717 Mya (4). Therefore, this anomaly cannot be mechanistically linked to the onset of glaciation as has been previously proposed (54–56). Moreover, none of these successions host any evidence for glaciation before the Islay anomaly.

Fire and Ice Revisited

The Sr isotope data reported here at ~ 732 Ma—as low as ~ 0.7064 in the Coppercap Formation—are consistent with other low pre-Sturtian values recorded in strata from Svalbard and Greenland (52, 53) and are less radiogenic than the ~ 780 -Mya values from Svalbard (57). Interestingly, Nd isotope studies have also suggested an increase to more mantle-like (more radiogenic) values tens of millions of years before the Sturtian glaciation (57). These data are consistent with the Fire and Ice hypothesis (58, 59), which proposes that Cryogenian glaciations were initiated through enhanced CO_2 consumption via weathering of basalts emplaced at low latitudes. The low-latitude breakup of Rodinia is thought to have been associated with the development of juvenile volcanic rift margins and the emplacement of multiple large igneous provinces (e.g., Willouran, Guibe, Gunbarrel, and Franklin large igneous provinces) (60). Enhanced volcanism and weathering of mafic material would have driven the ocean towards more unradiogenic Sr values and mantle-like Os_i values and a cooler global climate (Fig. 4), analogous to scenarios proposed for Mesozoic ocean anoxic events and Cenozoic cooling episodes (61–63).

In sharp contrast, the Os_i data from the overlying Twitya Formation yield a radiogenic signal for the postglacial ocean with the basal cap limestone recording an Os_i value of 1.44. From this initial high, values decline rapidly reaching a nadir of 0.42 at a height 2.6 m above the diamictite and then become steadily more radiogenic to a value of 0.62 before stabilizing to values ~ 0.50 above 10 m (Fig. 2). Similarly, Sr isotope values decrease from 0.7068 to 0.7066 in the lower 3 m and continue to fluctuate up-section before leveling out between 0.7068 and 0.7070. We interpret the signal recorded in the lower 3 m to represent the highly radiogenic, unmixed glacial melt water plume (64) and a subsequent decrease to less radiogenic Sr isotope values at 3–10 m to reflect the transgression of glacial deep waters (65). Up-section, it appears as though rapid mixing obscures the melt water signal; however, enhanced silicate weathering continued through the transgression in a high $p\text{CO}_2$ environment, resulting in an Os_i much more radiogenic than preglacial values, complementing the radiogenic trend recorded in the coeval Sr composition of seawater (Fig. 2). The absence of a trend to unradiogenic Sr isotope values across Cryogenian glacial deposits led some workers to conclude that Neoproterozoic glaciations were short lived (< 1 My) (66). However, this approach neglects

carbonate dissolution in response to ocean acidification and assumes that the Sr cycle is in steady state (67, 68), which is inconsistent with the sharp rise seen in globally distributed cap carbonate deposits.

Sr isotope data from Sturtian cap limestones in Namibia, Mongolia, and northwest Canada agree to the fourth decimal place (69, 70), thereby supporting a global correlation of this trend (Fig. 4). These Sr values increase rapidly from 0.7066 to 0.7072 in the Sturtian cap carbonate sequence and then flat-line through the rest of the Cryogenian period. Thus, the Neoproterozoic rise in seawater Sr isotope values may not have been gradual, as previously suggested (52), but stepwise and driven by extreme weathering in a postglacial supergreenhouse.

Conclusions

The geological record suggests that the Earth's climate system can exist in two climatic equilibria: one globally glaciated and the other not (46, 47). However, both the processes that maintain a steady climate and the drivers of long-term (> 10 My) climate change have remained obscure. Following a billion years of relative climatic stability with no apparent glacial deposits, the Neoproterozoic witnessed the transition from an ice-free world to a Snowball Earth. The unique Os and Sr isotope stratigraphy coupled with the Re-Os geochronology data presented herein also point towards a tectonic driver for long-term climate change and that the change in global weatherability may have been driven by a relative increase in juvenile, mantle-derived material weathered into the oceans from the continents.

Initiation of a Snowball Earth through a change in global weatherability has been criticized on the grounds that these background conditions should have persisted on a > 10 -My timescale, and after deglaciation the Earth should have rapidly returned to a Snowball state (46). Our new constraint of an ~ 55 -My duration of the Sturtian glacial epoch in northwest Canada is consistent with a short interlude between the Sturtian and Marinoan glaciations and a return to a glacial state on a time-scale consistent with enhanced weatherability (71). Increased input of mantle-derived material to the ocean would have also influenced geochemical cycles and promoted anaerobic respiration, potentially providing additional feedbacks that conspired to initiate a Neoproterozoic Snowball Earth (54). Our results confirm that the Sturtian glacial epoch was long lasting, its onset was accompanied by basalt-dominated weathering, and its termination was globally synchronous and followed by extreme weathering of the continents. The post-Sturtian weathering event may have in turn provided limiting nutrients like phosphorous to the ocean (72), leading to an increase in atmospheric oxygen and the radiation of large animals with high metabolic demands.

ACKNOWLEDGMENTS. We thank Rigel Lustwerk for providing samples from the 6YR core. We are grateful to the Yukon Geological Survey, Roger Summons, and Massachusetts Institute of Technology's National Aeronautics and Space Administration Astrobiology Institute node for support. We thank Roger Summons, Sam Bowring, and Dan Schrag for the use of their laboratories. We acknowledge the superb teams at Canadian and Fireweed helicopter companies and Dugald Dunlop from Meridian Mining via Colorado Minerals. We thank three reviewers and Paul Hoffman for comments on the manuscript and editorial advice. The Durham Laboratory for Source Rock Geochronology and Geochemistry is partially funded by TOTAL and BP. C.H. was supported by the Agouron Institute.

- Hoffman PF, Kaufman AJ, Halverson GP, Schrag DP (1998) A neoproterozoic snowball earth. *Science* 281(5381):1342–1346.
- Hoffman PF, Schrag DP (2002) The snowball Earth hypothesis; testing the limits of global change. *Terra Nova* 14(3):129–155.
- Halverson GP, Hoffman PF, Schrag DP, Maloof AC, Rice AHN (2005) Toward a Neoproterozoic composite carbon-isotope record. *Geol Soc Am Bull* 117(9-10):1181–1207.
- Macdonald FA, et al. (2010) Calibrating the Cryogenian. *Science* 327(5970):1241–1243.
- Kendall BS, Creaser RA, Calver CR, Raub TD, Evans DAD (2009) Correlation of Sturtian diamictite successions in southern Australian and northwestern Tasmania by Re-Os

- black shale geochronology and the ambiguity of "Sturtian"-type diamictite-cap carbonate pairs as chronostratigraphic marker horizons. *Precambrian Res* 172:301–310.
- Kendall BS, Creaser RA, Selby D (2006) Re-Os geochronology of postglacial black shales in Australia: Constraints on the timing of "Sturtian" glaciation. *Geology* 34:729–732.
- Ravizza G, Peucker-Ehrenbrink B (2003) The marine $^{187}\text{Os}/^{188}\text{Os}$ record of the Eocene-Oligocene transition: The interplay of weathering and glaciation. *Earth Planet Sci Lett* 210:151–165.
- Raymo ME, Ruddiman WF (1992) Tectonic forcing of late Cenozoic climate. *Nature* 359:117–122.

9. Paquay FS, Ravizza G (2012) Heterogeneous seawater $^{187}\text{Os}/^{188}\text{Os}$ during the Late Pleistocene glaciations. *Earth Planet Sci Lett* 349:126–138.
10. Dudás FO, Lustwerk RL (1997) Geochemistry of the Little Dal basalts: Continental tholeiites from the Mackenzie Mountains, Northwest Territories, Canada. *Can J Earth Sci* 34:50–58.
11. Jefferson CW, Parrish R (1989) Late Proterozoic stratigraphy, U/Pb zircon ages and rift tectonics, Mackenzie Mountains, northwestern Canada. *Can J Earth Sci* 26:1784–1801.
12. Harlan SS, Heaman LM, LeCheminant AN, Premo WR (2003) Gunbarrel mafic magmatic event: A key 780 Ma time marker for Rodinia plate reconstructions. *Geology* 31:1053–1056.
13. Chartrand FM, Brown AC (1985) The diagenetic origin of stratiform copper mineralization, Coates Lake, Redstone Copper belt, NWT, Canada. *Econ Geol* 80:325–343.
14. Lustwerk RL (1990) Geology and geochemistry of the Redstone strataform copper deposit, Northwest Territories, Canada. PhD thesis (Pennsylvania State Univ, University Park, PA).
15. Helmstaedt H, Eisebacher GH, McGregor JA (1979) Copper mineralization near an intra-Rapitan unconformity, Nite copper prospect, Mackenzie Mountains, Northwest Territories, Canada. *Can J Earth Sci* 16:50–59.
16. Eisebacher GH (1978) *Redefinition and Subdivision of the Rapitan Group, Mackenzie Mountains* (Geological Survey of Canada, Ottawa), pp 1–21.
17. Hoffman PF, Halverson GP (2011) Neoproterozoic glacial record in the Mackenzie Mountains, northern Canadian Cordillera. *The Geological Record of Neoproterozoic Glaciations*, eds Arnaud E, Halverson GP, Shields-Zhou G (The Geological Society, London), Vol 36, pp 397–412.
18. Klein C, Beukes NJ (1993) Sedimentology and geochemistry of the glaciogenic late Proterozoic Rapitan iron-formation in Canada. *Econ Geol* 84:1733–1774.
19. Eisebacher GH *Sedimentary Tectonics and Glacial Record in the Windermere Supergroup, Mackenzie Mountains, Northwestern Canada* (Geological Survey of Canada, Ottawa), pp 1–40.
20. Park JK (1997) Paleomagnetic evidence for low-latitude glaciation during deposition of the Neoproterozoic Rapitan Group, Mackenzie Mountains, N.W.T., Canada. *Can J Earth Sci* 34:34–49.
21. Aitken JD (1991) *The Ice Brook Formation and Post-Rapitan, Late Proterozoic glaciation, Mackenzie Mountains, Northwest Territories* (Geological Survey of Canada, Ottawa), Vol 404, pp 1–43.
22. James NP, Narbonne GM, Kyser TK (2001) Late Neoproterozoic cap carbonates: Mackenzie Mountains, northwestern Canada: Precipitation and global glacial melt-down. *Can J Earth Sci* 38(8):1229–1262.
23. Calver CR, et al. (2013) Globally synchronous Marinoan deglaciation indicated by U-Pb geochronology of the Cottons Breccia, Tasmania, Australia. *Geology* 41:1127–1130.
24. Johnston DT, Macdonald FA, Gill BC, Hoffman PF, Schrag DP (2012) Uncovering the Neoproterozoic carbon cycle. *Nature* 483(7389):320–323.
25. Young GM (1976) Iron-formation and glaciogenic rocks of the Rapitan Group, Northwest Territories, Canada. *Precambrian Res* 3:137–158.
26. Young GM (1982) The late Proterozoic Tindir Group, east-central Alaska; Evolution of a continental margin. *Geol Soc Am Bull* 93:759–783.
27. Denyszyn SW, Halls HC, Davis DW, Evans DAD (2009) Paleomagnetism and U-Pb geochronology of Franklin dykes in High Arctic Canada and Greenland: A revised age and paleomagnetic pole for constraining block rotations in the Nares Strait region. *Can J Earth Sci* 46:689–705.
28. Peucker-Ehrenbrink B, Ravizza G (2000) The marine osmium isotope record. *Terra Nova* 12:205–219.
29. Meisel T, Walker RJ, Irving AJ, Lorand J-P (2001) Osmium isotopic compositions of mantle xenoliths: A global perspective. *Geochim Cosmochim Acta* 65:1311–1323.
30. Jefferson CW (1978) *The Upper Proterozoic Redstone Copper Belt, Mackenzie Mountains, Northwest Territories*. PhD thesis (Univ of Western Ontario, London, Canada).
31. Brand U (2004) Carbon, oxygen and strontium isotopes in Paleozoic carbonate components: An evaluation of original seawater-chemistry proxies. *Chem Geol* 204:23–44.
32. Li D, Shields-Zhou G, Ling HF, Thirwall M (2011) Dissolution methods for strontium isotope stratigraphy: Guidelines for the use of bulk carbonate and phosphorite rocks. *Chem Geol* 290:133–144.
33. Derry LA, Keto LS, Jacobsen SB, Knoll AH, Swett K (1989) Sr isotopic variations in Upper Proterozoic carbonates from Svalbard and East Greenland. *Geochim Cosmochim Acta* 53(9):2331–2339.
34. Banner JL, Hanson GN (1990) Calculation of simultaneous isotopic and trace element variations during water-rock interaction with application to carbonate diagenesis. *Geochim Cosmochim Acta* 54:3123–3137.
35. Fanning CM, Link PK (2008) Age constraints for the Sturtian glaciation: Data from the Adelaide Geosyncline, South Australia and Pocatello Formation Idaho, USA. *Neoproterozoic extreme climates and the origin of early metazoan life*, eds Gallagher SJ, Wallace MW. *Selwyn Symposium* (Geological Society of Australia), pp 57–62.
36. Zhou C, et al. (2004) New constraints on the ages of Neoproterozoic glaciations in south China. *Geology* 32:437–440.
37. Calver CR, Black LP, Everard JL, Seymour DB (2004) U-Pb zircon age constraints on late Neoproterozoic glaciation in Tasmania. *Geology* 32(10):893–896.
38. Brasier MD, Shields G (2000) Neoproterozoic chemostratigraphy and correlation of the Port Askaig glaciation, Dalradian Supergroup of Scotland. *J Geol Soc London* 157:909–914.
39. Prave AR, Fallick AE, Thomas CW, Graham CM (2009) A composite C-isotope profile for the Neoproterozoic Dalradian Supergroup of Scotland and Ireland. *J Geol Soc London* 166:1–13.
40. Rooney AD, Chew DM, Selby D (2011) Re-Os geochronology of the Neoproterozoic-Cambrian Dalradian Supergroup of Scotland and Ireland: Implications for Neoproterozoic stratigraphy, glaciation and Re-Os systematics. *Precambrian Res* 185:202–214.
41. Treagus JE (1969) The Lower Dalradian Kinlochlaggan Boulder Bed, central Scotland. *Earth Pre-Pleistocene Glacial Record*, eds Hambrey MJ, Harland WB (Cambridge Univ Press, Cambridge, UK), pp 637–639.
42. Evans RHS, Tanner PWG (1996) A late Vendian age for the Kinlochlaggan Boulder Bed (Dalradian)? *J Geol Soc London* 153:823–826.
43. Fanning CM, Link PK (2004) U-Pb SHRIMP ages of Neoproterozoic (Sturtian) glaciogenic Pocatello Formation, southeastern Idaho. *Geology* 32:881–884.
44. Keeley JA, Link PK, Fanning CM, Schmitz MD (2013) Pre- to synglacial rift-related volcanism in the Neoproterozoic (Cryogenian) Pocatello Formation, SE Idaho: New SHRIMP and CA-ID-TIMS constraints. *Lithosphere* 5(1):128–150.
45. Bowring SA, Grotzinger JP, Condon DJ, Ramezani J, Newall M (2007) Geochronologic constraints on the chronostratigraphic framework of the Neoproterozoic Huqf Supergroup, Sultanate of Oman. *Am J Sci* 307:1097–1145.
46. Pierrehumbert RT, Abbot DS, Voigt A, Koll D (2011) Climate of the Neoproterozoic. *Annu Rev Earth Planet Sci* 39:417–460.
47. Abbot DS, Voigt A, Koll D (2011) The Jormungand global climate state and implications for Neoproterozoic glaciations. *J Geophys Res* 116(D18103).
48. Frimmel HE, Klotzli US, Siegfried PR (1996) New Pb-Pb single zircon age constraints on the timing of Neoproterozoic glaciation and continental break-up in Namibia. *J Geol* 104:459–469.
49. Key RM, et al. (2001) The western arm of the Lufilian Arc in NW Zambia and its potential for copper mineralization. *J Afr Earth Sci* 33:503–528.
50. Xu B, et al. (2009) SHRIMP zircon U-Pb age constraints on Neoproterozoic Quruqtagh diamictites in NW China. *Precambrian Res* 168:247–258.
51. Macdonald FA, Strauss JV, Rose CV, Dudás FO, Schrag DP (2010) Stratigraphy of the Port Nolloth Group of Namibia and South Africa and implications for the age of Neoproterozoic iron formations. *Am J Sci* 310:862–888.
52. Halverson GP, Dudás FO, Maloof AC, Bowring SA (2007) Evolution of the $^{87}\text{Sr}/^{86}\text{Sr}$ composition of Neoproterozoic seawater. *Palaeogeogr Palaeoclimatol Palaeoecol* 256:103–129.
53. Fairchild IJ, Spiro B, Herrington PM, Song T (2000) Controls on Sr and C isotope compositions of Neoproterozoic Sr-rich limestones of East Greenland and North China. *Carbonate Sedimentation and Diagenesis in the Evolving Precambrian World*, eds Grotzinger JP, James NP (SEPM Special Publication, Tulsa, OK), Vol 67, pp 297–313.
54. Tziperman E, Halevy I, Johnston DT, Knoll AH, Schrag DP (2011) Biologically induced initiation of Neoproterozoic snowball-Earth events. *Proc Natl Acad Sci USA* 108(37):15091–15096.
55. Hoffman PF, et al. (2012) Cryogenian glaciations on the southern tropical paleomargin of Laurentia (NE Svalbard and East Greenland), and a primary origin for the upper Russoya (Islay) carbon isotope excursion. *Precambrian Res* 206:207:137–158.
56. Schrag DP, Berner RA, Hoffman PF, Halverson GP (2002) On the initiation of snowball Earth. *Geochem Geophys Geosyst* 3(6).
57. Halverson GP, Wade BP, Hurtgen MT, Barovich KM (2010) Neoproterozoic Chemostratigraphy. *Precambrian Res* 182(4):337–350.
58. Donnadieu Y, Goddés Y, Ramstein G, Nédélec A, Meert J (2004) A 'snowball Earth' climate triggered by continental break-up through changes in runoff. *Nature* 428(6980):303–306.
59. Goddés Y, et al. (2003) The Sturtian 'snowball' glaciation: Fire and ice. *Earth Planet Sci Lett* 6648:1–12.
60. Li ZX, et al. (2008) Assembly, configuration, and break-up history of Rodinia: A synthesis. *Precambrian Res* 160(1–2):179–210.
61. Ravizza G, Peucker-Ehrenbrink B (2003) Chemostratigraphic evidence of Deccan volcanism from the marine osmium isotope record. *Science* 302(5649):1392–1395.
62. Turgeon SC, Creaser RA (2008) Cretaceous oceanic anoxic event 2 triggered by a massive magmatic episode. *Nature* 454(7202):323–326.
63. Kent DV, Mutttoni G (2013) Modulation of Late Cretaceous and Cenozoic climate by variable drawdown of atmospheric $p\text{CO}_2$ from weathering of basaltic provinces on continents drifting through the equatorial humid belt. *Climates of the Past* 9:525–546.
64. Shields G (2005) Neoproterozoic cap carbonates: A critical appraisal of existing models and the plume world hypothesis. *Terra Nova* 17(4):299–310.
65. Hoffman PF, et al. (2007) Are basal Ediacaran (635 Ma) post-glacial "cap dolostones" diachronous? *Earth Planet Sci Lett* 258:114–131.
66. Jacobsen S, Kaufman AJ (1999) The Sr, C, and O isotopic evolution of Neoproterozoic seawater. *Chem Geol* 161:37–57.
67. Le Hir G, Ramstein G, Donnadieu Y, Goddés Y (2008) Scenario for the evolution of atmospheric $p\text{CO}_2$ during a snowball Earth. *Geology* 36:47–50.
68. Higgins JA, Schrag DP (2003) Aftermath of a snowball Earth. *Geophysics, Geochemistry, Geosystems* 4:1–20.
69. Yoshioka H, Asahara Y, Tojo B, Kawakami S (2003) Systematic variations in C and Sr isotopes and elemental concentrations in Neoproterozoic carbonates in Namibia: Implications for a glacial to interglacial transition. *Precambrian Res* 124:69–85.
70. Shields G, Brasier MD, Stille P, Dorjnamjaa D (2002) Factors contributing to high $\delta^{13}\text{C}$ values in Cryogenian limestones of western Mongolia. *Earth Planet Sci Lett* 196:99–111.
71. Mills B, Watson AJ, Goldblatt C, Boyle RA, Lenton TM (2011) Timing of Neoproterozoic glaciations linked to transport-limited global weathering. *Nat Geosci* 4:861–864.
72. Planavsky NJ, et al. (2010) The evolution of the marine phosphate reservoir. *Nature* 467(7319):1088–1090.